RSC Advances

ROYAL SOCIETY OF CHEMISTRY

www.rsc.org/advances

Synergistic effect of graphene and ionic liquid containing phosphonium on the thermal stability and flame retardancy of polylactide

Haoguan Gui [a], Pei Xu [a,b*], Yadong Hu [a],Jie Wang [a], Xuefeng Yang [a], Ali Bahader [a], Yunsheng Ding [a,b*]

[a] *Department of Polymer Science and Engineering, Hefei University of Technology, Hefei, 230009 , P. R. China.*

[b] *Anhui Key Laboratory of Advanced Functional Materials and Devices, Hefei University of Technology, Hefei, 230009, China.*

Corresponding author Tel: +86 551 62901545;

E-mail: Pei Xu (chxuper@hfut.edu.cn);

Yunsheng Ding (dingys@hfut.edu.cn)

Abstract

A series of nanocomposites based on the biodegradable plastic, polylactide (PLA), have been prepared by melt-blending with graphene (Gra) and ionic liquid containing phosphonium ([PCMIM]PF_6, IL) surface-functionalized graphene (GIL). The morphology, mechanical properties, thermal stability and burning behaviour of composites were investigated by Field Emission Scanning Electron Microscopy (FESEM), Tensile Test, Impact Test, Thermogravimetric Analysis (TGA), Limiting Oxygen Index (LOI), UL-94 Test and Cone Calorimeter Test (CCT), respectively. Surface morphology and chemical structure of the char residues were explored by FESEM and Raman spectroscopy. It is confirmed that the fire-retardant performance of PLA/GIL composites was significantly improved compared to PLA/IL and PLA/Gra; the CCT data showed reduction in heat release rate and total heat released with increase of the char residue from TGA results. It revealed that the catalytic charring effect of ionic liquid, the physical isolating effect of graphene, and the combined effect of both ionic liquid and graphene (forming continuous and compact char layers) were very efficient in improving the flame retarding properties of PLA/GIL nanocomposites.

1. Introduction

Polylactide (PLA) is attracting increasing attention in industry because PLA is biodegradable aliphatic polyester with high mechanical strength, thermal plasticity, high melting point, high degree of transparency, and ease of fabrication, which can be used in biomedical fields, household engineering and packing industry, etc. The major drawback of PLA is its low thermal stability, high combustibility and melts dripping, which extremely limits its applications in electrical industry and building materials.[1, 2] Therefore, the improvement of thermal stability and flame retarding performance of PLA has been an important and urgent task. Therefore, modification for flame retardancy of PLA is necessary.

Recently, graphene has been taking place gradually in fire safety applications in terms of polymer nanocomposites due to its high thermal stability and forming a physical barrier between polymer and graphene during the combustion of the nanocomposites.[3-6] However, the graphene layers have strong cohesive interaction which makes them difficultly dispersible.[7] To reduce the cohesive force between the graphene sheets and also to improve flame retardancy of composites by grafting various flame retardants at same time is very much essential.[8-11] Hu et al. utilized organic phosphate, phenyl dichlorophosphate (PDCP), to functionalize graphene oxides (GO) and incorporate into epoxy resin (EP) matrix, which proved better flame retardant properties than EP/GO composites.[8] As reported by Song et al., graphene oxide functionalized with hexachlorocyclotriphosphazene (HCCP, molecular formula: $P_3N_3Cl_6$) and hydroxyethyl acrylate (HEA) can decrease peak heat release rate, thermal degradation rate and total heat release of polystyrene (PS).[9] Poly(piperazine spirocyclic pentaerythritol bisphosphonate) (PPSPB) has been covalently grafted onto the surfaces of graphene oxide, which can improve thermal stability and reduce obviously the flammability of ethylene vinyl acetate copolymer (EVA).[10] Similarly, polyphosphamide (PPA), was grafted onto the surface of graphene nanosheets by Hu et al., and the functionalized graphene was incorporated into EP to enhance the fire resistance of the polymer nanocomposites.[11]

Ionic liquids (ILs) are organic salts with low melting temperatures, typically below 100 °C, since their asymmetric structure, consisting of a large organic cation combined with a usually smaller size anion. They, exhibiting low viscosity, high thermal and air stability, good electrical conductivity, low vapor

pressure and apparent nonflammability, are developing the application of polymeric materials.[12, 13] Furthermore, some ILs with functional groups can behave as effcient catalysts in some reactions or processes.[14, 15] Li et al. prepared a kind of ionic liquids ($[BMIm]_3PMo$) composed of 12-phosphomolbdic acid (PMoA) based 1-butyl-3-methylimidazolium ([BMIm]) and introduced into intumescent flame retardant polypropylene (PP/IFR). The PP composite with 14.5 *wt*. % IFR and 0.5 *wt*. % IL (IL was thought as a catalyst on the cross-linking and char forming reaction of PP at higher temperature) can pass the UL-94 V-0, while that for the single IFR is more than 25 *wt*. %.[16] They also reported other two kind ionic liquids, containing 12-phosphotungstic acid (PWA) and 12-silicotungstic acid (SiWA), showed poorer synergistic effects on charring behaviour. [17] Our previous works have also indicated that the ionic liquid containing phosphorus ([PCMIM]Cl) could greatly promote the char formation of PP/IFR composites, and endow the composites with satisfying processability and mechanical properties.[18] According to the reports, ILs containing flame retardant elements and structures would be potential flame retardants or flame-retarded synergistic agents for polymer composites.

Additionally, varieties of groups have reported imidazolium-based ionic liquids (Imi-ILs) as alternative polar solvents for graphene dispersion since Fukushima and co-workers successfully uniformly dispersed carbon nanotubes by using Imi-ILs,[19-21] forming a possible "π-π and/or cation-π" interactions between the π-electronic surfaces of carbon nanotubes and imidazolium cation of Imi-ILs.[22] This method is considered simple, environment friendly and effective one compared with the covalently methods mentioned above.[23] Furthermore, this non-covalently modified graphene have applied successfully to polymer composites.[24-26] Yang et al. used 1,6-bis[3-(vinyl benzyl)imidazolium-1-yl]hexane chloride (VbimBr) in the preparation of graphene/PMMA composites with large climb in storage modulus (+ 58.3%) and glass-transition temperature (T_g) (+ 19.2 °C) at 2.08 *vol*. % graphene loading.[24] Bermúdez and co-workers determined the effect of 1-octyl-3-methylimidazolium tetrafluorobotate modified graphene on the tribological performance of EP, showing low friction coefficients and negligible wear.[25] The ionic liquid (1-butyl-3-methylimidazolium tetrafluoroborate, $BmimBF_4$) functionalized graphene was applied to the preparation of molecular imprinting electrochemical sensor by Wang et al.[26]

This work aims to study the influence of the incorporation of graphene and especially surface-functionalized graphene with a novel ionic liquid containing phosphorus ([PCMIM]PF_6, shown in Fig.1) on the fire retardation behavior of PLA nanocomposites. The work focuses on the relationship between evolution of the microstructure of residue chars, thermal stability and flammability of composites during combustion. The mechanism of the synergistic effect between IL and graphene on improving the flame retardancy is discussed.

2. Experimental

2.1 Materials

PLA (grade 4032D) was purchased from Nature-Works LLC, USA, with 98.7 mol % *L*-isomeric content, and density of 1.24 g/cm^3. Graphene (5-15 μm in diameter, 3 nm thickness) were purchased from Ningbo Morsh Technology. Co., Ltd. [PCMIM]PF_6 was synthesized following a similar and optimized procedure compared with our previous work (the synthesizing procedure and confirmation of structure was shown in the Supplementary Information)[18].

2.2 Preparation of flame retarded PLA/Gra, PLA/GIL or PLA/GIL nanocomposites

The filler, surface-modified graphene with ionic liquid, was prepared by simple mechanical grinding (shown in Fig. 1)[19], the mass fraction ratio of graphene to ionic liquid is 1:3. The flame resistant nanocomposites, PLA/1Gra (1 *wt*. % graphene in the nanocomposites), PLA/3IL (3 *wt*. % IL in nanocomposites respectively) and PLA/2GIL, PLA/4GIL (2 *wt*. % and 4 *wt*. % modified graphene in nanocomposites respectively), were prepared by melt-blending, as follows: First, PLA was added in a Haake internal mixer operating at 175 °C and 60 rpm for pre-melting and then Gra , IL or GIL were added and mixed for another 8 min. The obtained products were further moulded to disk-shaped sheets for structure characterization and properties measurements by hot-pressing at about 180 °C under a pressure of 10 MPa. All materials were completely dried at predetermined temperature under vacuum before using, and the prepared samples were kept in desiccator. The schematic diagrams of the preparation of PLA/GIL nanocomposites are schematically shown in Fig. 1.

2.3 Characterization

The Raman spectroscopy was performed with a Raman spectrometer (LABRAM-HR), which is

equipped with an excitation wavelength of 514.5 nm. The thermogravimetric analysis (TGA) was done using TG 209 F3, Netzsch with a heating rate of 10 °C/min from room temperature to 800 °C under nitrogen atmosphere. Differential scanning calorimetry (DSC) measurements were performed using a Mettler-DSC (Switzerland) at a heating rate of 10 °C/min in a nitrogen atmosphere. The data reported were collected from the second scan. The procedure was as follows: Two scans from 20 to 190 °C were conducted, and the composites were cooled to 20 °C between the scans. The first scan was designed to erase the thermal history of the samples. The degree of crystallinity was determined by subtracting ΔH_c from ΔH_m and considering a melting enthalpy of 93 J/g for 100% crystalline PLA.[27] The fracture surfaces and char residues of the PLA/Gra and PLA/GIL composites were investigated by field emission scanning electron microscopy (FESEM, Hitachi-SU8020). All the fracture surfaces and char residues were sputter-coated with gold layer before examination. The tensile strength and elongation at break were measured on a C64 materials testing machine (SANS, China) with dumb-bell specimens' dimensions of 150 × 10 × 1 mm^3 according to ISO 527-3: 1995. The crosshead speed was 50 mm/min. Izod impact strength was measured by a JC-5D cantilever beam impact tester (Chengde, China) with strip specimens' dimensions of 100 × 10 × 4 mm^3 according to ISO 180: 2000. Both tensile test and impact test were measured six times, and the results were averaged to obtain a mean value. The limit oxygen index (LOI) values were measured on an HC-2C oxygen index meter (Jiangning, China) with sheet dimensions of 100 × 6.5 × 3 mm^3 according to ISO 4589-2: 1996. Burning behavior - vertical (UL-94) were conducted on a CZF-2 vertical burning test instrument (Jiangning, China) with sheet dimensions of 100 × 13 × 3mm^3 according to IEC 60695-11-10: 1999. The combustion parameters were measured according to ISO 5660 using a cone calorimeter (FTT Company, UK) at heat flux of 35 kW/m^2. All samples for the cone calorimeter measurements with the dimensions of 100×100×4 mm^3. The cone data presented were the averages of two replicated experiments.

3. Results and Discussion

3.1 Structural characteristics of graphene and GIL

Raman spectroscopy, usually used to characterize graphitic structure of materials, and to evaluate the order degree of carbon materials, is a powerful tool to quantify the transformations from sp^3 to sp^2 hybridization through the intensity variation of bands in the spectrum.[28] From the Raman spectrum (shown in Fig.2), two visible bands were observed, the peak around 1350 cm^{-1} is referred as D band

which originates from the significant defects or disorders in the nanostructures, and the second around 1594 cm^{-1} is assigned as G band which derives from the tangential vibrations of the carbon atoms, respectively.[29] The intensity ratio *R* (the intensity of D to G band) was calculated for symbolizing the degree of crystallinity and purity of graphene.[30] The decrease in the value of R for GIL (1.67) as opposed to raw graphene (1.54) is due to the rearrangement of the graphene in presence of ionic liquids that means the amorphous carbon materials and impurities have decreased by physical functionalizations.[31] A increase of the intensity of *R* in the spectra of GIL as compared to pristine graphene, is probably due to the cation–π/π–π interaction between ionic liquids and the graphene.[32] What's more, the interaction between IL and the graphene can also by the Fourier Transform Infrared Spectroscopy (FTIR) and X-ray Photoelectron Spectroscopy (XPS) (shown Fig. S4, Fig. S5 and Fig. S6).

3.2 Thermal properties of IL and GIL

Fig. 3 shows the TGA and derivative thermogravimetry (DTG) curves of IL and GIL. It can be seen that IL shows very high thermal stability. The initial decomposition temperature of IL is about 326.8 °C, based upon 5% weight loss. DTG curve of IL shows two peaks at 338.2 °C and 376.8 °C. The whole degradation course of [PCMIM]PF_6 can be divided into two stages. The decomposing temperature in the first step is between 282.3 °C and 369.3 °C, which may contribute to the disintegration of PEPA.[33] The second is ranging from 369.3 °C to 497.2 °C, possibly due to the pyrolysis of imidazolium salts.[34] Another important thing that should be mentioned is that IL has perfect ability of char formation and has residues of 46.8 *wt* % at 400 °C, 40.0 *wt* % at 600 °C and 39.7 *wt* % at 700 °C, respectively, implying that IL can be used as an efficient char forming agent. GIL exhibits a two-step degradation process and no weight loss is observed till 300°C. DTG curve of GIL shows two peaks at 351.4 °C and 374.1 °C. Compared to the first peak of IL, the GIL demonstrated an excellent shift in the decomposition temperature by 13.2 °C, since the surface modification of the graphene by IL enhance the physically interaction as well as thermal stability, without chemical impairment of graphene.[16]

3.3 Morphology of the nanocomposites

In order to further investigate the effect of IL on the dispersibility and compatibility of graphene in the PLA matrix, the morphology of the PLA composites was analyzed. All specimens were frozen in liquid

nitrogen for 15 min and then made to fracture in a sudden burst. The morphology of PLA/Gra and PLA/GIL nanocomposites was investigated by FESEM. The white wrinkled topography in Fig. 4 represents the ends of graphene stretched out of the PLA matrix. We can see that not only graphene and GIL are dispersed uniformly in PLA matrix but the distance between graphene also decreases with the introduction of the IL. These observations suggest that IL can improve the compatibility between graphene and PLA matrix, resulting in a uniform dispersion of GIL in PLA matrix. For the PLA/4GIL it can be clearly seen that graphene are coated by IL layers. The coating is fairly uniform, and no contour profile of the graphene was observed. This means that the interfacial bonding between graphene and PLA matrix greatly increases because of the incorporation of IL. As IL has low melt point, high melt flow ability and powerful interaction with graphene, it can well wet the surface of graphene and carry graphene into PLA phase, therefore effectively promoting the dispersion process.[35, 36] Such a thin flame-retardant IL shell should prevent the direct contact of graphene with each other when blended with PLA. Thus it can be inferred that layer formation of IL on the surface of the graphene will change the flammability properties of the composite material as discussed in the following section.

3.4 Mechanical properties of the nanocomposites

The mechanical properties of PLA PLA/1Gra, PLA/3IL or PLA/4GIL composites are summarized in Table 3. It can be found that the addition of Gra leads to increase of tensile strength of PLA, while the elongation at break and impact strength show a decrease with respect to PLA, which is confirmed as the reinforcing effect of graphene [37]. The presence of IL reduces tensile strength of PLA, while the elongation at break and impact strength of PLA/3IL are increased due to the plasticization of IL [38]. When 2 *wt* % GIL is added, the tensile strength, elongation at break and impact strength of PLA/2GIL are increased to 61 ± 2.1 MPa, 6.0 ± 1.3 % and 4.1 ± 1.0 kJ/m^2 respectively compared with PLA. It revealed that PLA/GIL composite presents considerable mechanical properties for application.

3.5 Thermal stability of the nanocomposites

TGA is an effective tool to evaluate thermal behavior of various polymers as well as their composites. The thermal stability of a polymeric material is very important when used as a flame retardant, which process mainly concerns the release of decomposition products and the formation of carbon residues[39]

Typical thermo-oxidative degradation temperatures, the onset degradation temperature which is evaluated by the temperature of 5 *wt* % weight loss ($T_{initial}$) and the temperature of the maximum weight loss rate (T_{max}), and the solid residue are summarized in Table 1. Thermal degradation behaviors of PLA and PLA nanocomposites in nitrogen condition are presented in Fig. 5, and the related data are listed in Table 1. The pure PLA starts to decompose at 318.8 °C and the thermal degradation process only has one stage. The char residue of pure PLA is 0.9 *wt* % at 700 °C, and the T_{max} appeared at a temperature of 351.1 °C. The PLA/1Gra composite starts to decompose at 324.9 °C and the thermal degradation process only has one stage. The stage occurs between 300 and 400 °C, corresponding to a strong DTG peak at 356.1 °C (T_{max}) and the weight loss is about 39.9 *wt* %. The char residue of PLA/1Gra composite is 3.4 *wt* % at 700 °C. As the graphene was added, the value of $T_{initial}$ and T_{max} is further increased, indicating that the PLA/1Gra composite have stronger thermal stabilities owing to the addition of graphene. However the thermal stability of PLA is decreasing with IL added in the composite, $T_{initial}$ and T_{max} drop to 307.5 °C and 335.8 °C, respectively. And the char residue climbs to 5.3 at 700 °C. These phenomena prove that the IL can catalyze the thermal degradation and char yield of PLA. For the PLA/GIL composites, the thermal degradation process of PLA/2GIL and PLA/4GIL has one stage that is at 300-400 °C. As the content of GIL increases, the $T_{initial}$ and T_{max} shift to a slightly higher temperature because of the good physical barrier effect of the GIL layers and the strong interfacial interactions between GIL and PLA.

The char formed during thermal degradation and combustion is important for fire safety applications. The char yield of PLA is 0.9 *wt* % at 700 °C, and the char yield of the PLA/1Gra composites is increased to 3.4 *wt* %. The residue amount of graphene and IL is approximately 95.1 *wt* % and 39.7 *wt* %. So in the char of PLA/1Gra (3.4 *wt* %), 1.0 *wt* % (1 *wt* %×95.1 *wt* %) is from Gra and the rest, 2.4 *wt* %, is from PLA. Therefore, the true char yield of PLA in PLA/1Gra is just upon 2.4 *wt* % (2.4 *wt* %/99.0 *wt* %), which is a near 3 times increase (2.4 *wt* %/0.9 *wt* %) as compared with neat PLA. In the char of PLA/3IL (5.3 *wt* %), 1.2 *wt* % (3 *wt* %×39.7 *wt* %) is from IL and the rest, 4.1 *wt* %, is from PLA. Therefore, the true char yield of PLA in PLA/3IL is upon 4.2 *wt* % (4.1 *wt* %/97.0 *wt* %), which is a near 4 times increase (4.2 *wt* %/0.9 *wt* %) as compared with neat PLA. However, the true char yield of the PLA in PLA/2GIL and PLA/4GIL is about 3.9 *wt* % (3.8 *wt* %/98.0 *wt* %) and 8.3 *wt* % (8.0 *wt* %/96.0 *wt* %), which is a more than 4 and 9 times increase as compared with neat PLA. So the char

yield was actually entirely from the incorporated graphene and no char was formed from the PLA in the PLA/1Gra composite. From these PLA/IL and PLA/GIL comparisons, it is clear that IL catalyzes the char formation of PLA.

It is clearly seen that all PLA/GIL composites decompose lately in comparison with pure PLA. Furthermore, at a temperature higher than 600 °C, the flame retardant PLA has more char residue than PLA. The above phenomena can be explained as follows. The phosphate group of IL would be would form pyrophosphoric acid at lower temperature, which can link graphene as a network structure. And the volatile combustible fragments generated during polymer degradation are prevented from diffusing towards the surface of the burning polymer and feeding the flame.[40-43] As a result, GIL improves the thermal stability of the PLA composites at higher temperature and promotes the formation of char layer. Additionally, the thermo-oxidative degradation curves of neat PLA and the nanocomposites experimented under the air atmosphere for comparing the degradation under different gas condition is shown in Fig. S7.

3.6 Thermal behaviour of the nanocomposites

Fig. 6 presents the DSC thermograms of different PLA nanocomposites during the second DSC heating cycle. The results are summarized in Table 2. The specific thermal properties of the PLA matrix are altered after addition of graphene and IL. The glass transition temperature (T_g) and the melting temperature (T_{m1} and T_{m2}) of pure PLA are 60.4, 165.4 and 169.6 °C, respectively, and an obvious broad cold crystallization (T_c) peak is found. The amplitude of T_g depression lies between 60.4 °C (T_g of PLA) and 58.6 °C (T_g of PLA/3IL), suggesting IL have an effect on plasticizing. What is more, the cold crystallization peak for PLA/3IL is much narrower compared with PLA, indicating that the existence of IL can increase the crystallization rate of PLA to a certain extent. The addition of graphene or GIL slightly increases the glass transition temperatures of the composites, and the melting temperatures are slightly decreased. Obvious sharp cold crystallization temperature peaks are observed in the composites and the cold crystallization temperature value of the PLA/2GIL and PLA/4GIL slightly decreases compared with those of PLA/1Gra. It comes out that pure PLA exhibits the lower crystallinity degree (28.2 %) than that of PLA/1Gra (32.5 %), and the incorporation of GIL further leads to increased crystallinity, i.e., 36.8, and 37.3 % for PLA/2GIL, PLA/4GIL, respectively. The

addition of GIL into PLA acts as a nucleating agent, giving rise to the significant increases in crystallinity of the PLA composites.[44] The double melting peaks of PLA composites are attributed to the lamellar reorganization, and the melting peaks located at the lower temperature are ascribed to less-organized crystals.

3.7 Flammability properties of the nanocomposite

From LOI data, pure PLA is a flammable polymeric material, and its LOI value is only 19. While the LOI value of PLA/3IL, PLA/1Gra, PLA/2GIL and PLA/4GIL increases to 25, 22 25 and 28, respectively. From UL-94 results, pure PLA is highly combustible and is not classified in the UL-94 rating. The PLA/3IL, PLA/1Gra, PLA/2GIL and PLA/4GIL reach V1, V2, V1 and V1 rating. From the above result, it can be concluded that GIL is a effective carbonization agent for PLA, which can promote the formation of the protective char layer, so the flame retardant properties of PLA nanocomposites improve.

The cone calorimeter is a performance-based bench scale fire testing apparatus and provides a wealth of information on combustion behavior.[45] Fig. 7(a) shows curves of the heat release rate (HRR) against time of PLA, PLA/Gra, PLA/IL and PLA/GIL composite. The detailed data is shown in Table 4. It can be seen that the material without flame retardant burns very fast after ignition and a sharp HRR peak appears with a p_{HRR} value of 324 kW/m^2. When graphene is incorporated into the matrix alone (PLA/1 Gra), the p_{HRR} and Av_{HRR} is reduced to 214 kW/m^2 and 86 kW/m^2. When IL is incorporated into the matrix alone (PLA/3IL), the p_{HRR} and Av_{HRR} is reduced to 168 kW/m^2 and 75 kW/m^2. With the combination of graphene with IL (PLA/2GIL), the p_{HRR} and Av_{HRR} was decreased to 141 kW/m^2 and 67 kW/m^2. In particular, the p_{HRR} and Av_{HRR} of PLA/2GIL is little than that of PLA/3IL.

PLA, PLA/Gra, PLA/IL and PLA/GIL nanocomposite also showed considerable differences in the total heat release (THR) curves presented in Fig. 7(b). At the end of burning, neat PLA has released a total heat of 49 MJ/m^2, the PLA/1Gra has released to 46 MJ/m^2, the PLA/3IL has released to 43 MJ/m^2, whereas only 40 and 33 MJ/m^2 has been released by the PLA/2GIL and PLA/4GIL composite respectively. This latter significant difference results from the addition of IL to the polymer, and indicates that a part of the polymer was not completely burnt because while burning, an intumescent

char was formed on the surface of the matrix. The result suggested that the IL has better performance when used as a charring agent in GIL formulations. The positive effect between graphene and IL may lead to the formation of higher quality char layer during combustion for PLA/GIL. This char layer protects the matrix effectively from heat penetrating and hence prevents its further degradation.[40-43]

The time to ignition (TTI) of virgin PLA is 88 s, while those of PLA/GIL composite shift to an earlier time. This phenomenon could be explained as that the high thermal conductivity of graphene-based materials speeds up the heat conducting from the surface into the graphene-based composites, PLA is sensitive to the acid species that result from the pyrolysis products of GIL, and thereby the addition of IL catalyzes the degradation of PLA and brings the TTI value forward.

3.8 Digital photos of the nanocomposite after CCT

Comparing the results of thermal properties and flammability properties of the materials in this study, we can conclude that the flammability properties of PLA/GIL composites are strongly affected by the physical barrier of graphene, and the char-forming and the high catalytic activity of the IL. The results of the investigation of morphologies and structure of residues of the composites after combustion provide other useful information about the flame retardation mechanism of the above nanocomposites. Fig. 8 shows macro-morphologies of the final chars after CCT of PLA/Gra, PLA/IL and PLA/GIL nanocomposites. In the case of neat PLA, the material was completely burned and no char was obtained. For PLA/1Gra and PLA/3IL composite, many big, black discrete islands are formed at the end of the test. For PLA/2GIL and PLA/4GIL samples, cohesive, uniform, and even partially foamed carbonaceous residue are left at the end of the test. This better cohesion of the combustion residue of the composite based on GIL could be explained by the individually dispersed modified graphene forming a rigid network between graphene and IL. The incorporation of Gra/IL leads to the increase of char yield and the formation of a continuous and compact char layer, which is consistent with the TGA result. The cohesive and dense char surface as an effect barrier can inhibit the degradation products, heat, and oxygen transfer to protect the underlying polymers.

3.9 Morphology investigation of the char residues

Fig. 9 shows the FESEM images of the residues of PLA/Gra, PLA/IL and PLA/GIL nanocomposites,

respectively. It can be seen that PLA/1Gra and PLA/3IL shows a network structure consisting of bundled, inter-wined graphene and there are many pores and microcracks within the network after combustion. Comparing the smooth surface of PLA/1Gra after combustion, the cracks and holes in the PLA/3IL became fewer and the porous and incompact surface changed into a more compact one.

However, the char of PLA/2GIL and PLA/4GIL shows totally different morphology. The char structure of PLA/GIL is more compact and more chars are left for wrapping the graphene. Due to the excellent intumescent effect of IL and strong interaction between IL and graphene, some graphene acts as the 'bridge' and overlaps the intumescence between IL.[11] It could be seen that the surface of the char residue is continuous, compact and unsmoothed, and the network formed by the coated graphene is clearly surrounded by char residue. The thickness of the graphene for the residue of PLA/4GIL is even larger than that of PLA/2GIL before burning. This may be the reason why the final network structure of PLA/4GIL is more compact than that of PLA/2GIL. The composited char surface could provide a reinforced char layer with a high quality leading to low amount of volatiles. In summary, the improved flame retardancy property was attributed to excellent synergistic effect between IL and graphene which can improve both the dispersion of graphene in polymer matrix and flame retardancy of the composites.

3.10 Raman spectra for the char residues

Fig. 10 presents the Raman spectra of the char residue for different flame-retardant samples after CCT. *R* values of the char residue for the PLA/2GIL and PLA/4GIL composites decreased from 0.86 to 0.75 and 0.58, respectively, in comparison with PLA/1Gra when IL was incorporated, indicating that a more graphitic structure formed.[46] Thus, it is reasonably believed that the improved flame resistant properties of the PLA/GIL composite are attributed to the synergistic effect of IL and the physical barrier effect of graphene. During the combustion process, IL may act to catalyze the carbonization of the degradation products. Meanwhile, graphene can function as a physical barrier to absorb degradation products. Degradation products continually collect on the graphene, which serves as a template for the formation of microchar. Furthermore, the degradation products are catalytically converted into char by the combination of the physical barrier effect of graphene and the catalytic effect of IL.

Therefore, one could conclude that IL and graphene could both transfer amorphous char into graphitic

structure after the material was ignited. Thus, the strength of char layer was enhanced and became more compact, performing a better barrier effect during combustion. It can be concluded that a higher graphitization degree in the char structure tends to give better protection of materials from thermal oxidation.

4. Conclusions

The flame resistance properties of the PLA/Gra and PLA/GIL composites were investigated by cone calorimeter, which revealed that incorporation of IL containing phosphonium and graphene was very efficient in improving the flame retardance of PLA composite. The morphology, flame retardance and thermal stability of the PLA composites were comprehensively investigated. In details, HRR and THR of PLA composite was significantly decreased compared to those of neat PLA during combustion. Raman spectra of the char residue after cone calorimetry confirmed that the incorporation of IL enhanced the formation of an ordered graphitic structure, compared with PLA/Gra composite. SEM observation suggested that the char residue for the PLA/4GIL composite was much more continuous and compact than that of PLA/2GIL composite. The fire retardant mechanism observed in the cone calorimeter is char formation, slowing the initial decomposition, and increasing the final char yield. This may be related to the obvious synergistic effect between IL and graphene, and the formation of a continuous and compact char layer of GIL, which can reduce the transfer of heat and fuel in the burning process. At the same time, the IL in the nanoparticle might catalyse the reaction and form char layer leading to graphitization.

Acknowledgments

This research was supported by the National Natural Science Foundation of China (51373045) and the Anhui Provincial Natural Science Foundation (1308085QB40).

Notes and references

[a] *Department of Polymer Science and Engineering, Hefei University of Technology, Hefei, 230009 , P. R. China.*

[b] *Anhui Key Laboratory of Advanced Functional Materials and Devices, Hefei University of Technology, Hefei, 230009, China.*

Corresponding author Tel: +86 551 62901545;

E-mail: Pei Xu (chxuper@hfut.edu.cn);

Yunsheng Ding (dingys@hfut.edu.cn)

† Electronic Supplementary Information (ESI) available: [details of any supplementary information available should be included here]. See DOI: 10.1039/b000000x/

1. L. Yu, K. Dean and L. Li, *Progress in Polymer Science*, 2006, **31**, 576-602.
2. R. M. Rasal, A. V. Janorkar and D. E. Hirt, *Progress in Polymer Science*, 2010, **35**, 338-356.
3. X. Wang, L. Song, H. Yang, H. Lu and Y. Hu, *Industrial & Engineering Chemistry Research*, 2011, **50**, 5376-5383.
4. P. a. Song, Y. Yu, T. Zhang, S. Fu, Z. Fang and Q. Wu, *Industrial & Engineering Chemistry Research*, 2012, **51**, 7255-7263.
5. X. Wang, L. Song, H. Yang, W. Xing, H. Lu and Y. Hu, *Journal of Materials Chemistry*, 2012, **22**, 3426-3431.
6. J. Zhu, M. Chen, Q. He, L. Shao, S. Wei and Z. Guo, *RSC Advances*, 2013, **3**, 22790-22824.
7. R. K. Layek and A. K. Nandi, *Polymer*, 2013, **54**, 5087-5103.
8. Y. Guo, C. Bao, L. Song, B. Yuan and Y. Hu, *Industrial & Engineering Chemistry Research*, 2011, **50**, 7772-7783.
9. C. Bao, Y. Guo, B. Yuan, Y. Hu and L. Song, *Journal of Materials Chemistry*, 2012, **22**, 23057-23063.
10. G. Huang, S. Chen, S. Tang and J. Gao, *Materials Chemistry and Physics*, 2012, **135**, 938-947.
11. X. Wang, W. Xing, X. Feng, B. Yu, L. Song and Y. Hu, *Polymer Chemistry*, 2014, **5**, 1145-1154.
12. R. D. Rogers and K. R. Seddon, *Science*, 2003, **302**, 792-793.
13. P. Kubisa, *Progress in Polymer Science*, 2004, **29**, 3-12.
14. C. Yue, D. Fang, L. Liu and T.-F. Yi, *Journal of Molecular Liquids*, 2011, **163**, 99-121.
15. Q. Zhang, S. Zhang and Y. Deng, *Green Chemistry*, 2011, **13**, 2619-2637.
16. S. Chen, J. Li, Y. Zhu, Z. Guo and S. Su, *Journal of Materials Chemistry A*, 2013, **1**, 15242-15246.
17. S. Chen, J. Li, Y. Zhu and S. Su, *RSC Advances*, 2014, **4**, 32902-32913.

18. X. Yang, N. Ge, L. Hu, H. Gui, Z. Wang and Y. Ding, *Polymers for Advanced Technologies*, 2013, **24**, 568-575.
19. T. Fukushima, A. Kosaka, Y. Ishimura, T. Yamamoto, T. Takigawa, N. Ishii and T. Aida, *Science*, 2003, **300**, 2072-2074.
20. T. Fukushima and T. Aida, *Chemistry – A European Journal*, 2007, **13**, 5048-5058.
21. T. Sekitani, Y. Noguchi, K. Hata, T. Fukushima, T. Aida and T. Someya, *Science*, 2008, **321**, 1468-1472.
22. J. C. Ma and D. A. Dougherty, *Chemical Reviews*, 1997, **97**, 1303-1324.
23. R. Peng, Y. Wang, W. Tang, Y. Yang and X. Xie, *Polymers*, 2013, **5**, 847-872.
24. Y.-K. Yang, C.-E. He, R.-G. Peng, A. Baji, X.-S. Du, Y.-L. Huang, X.-L. Xie and Y.-W. Mai, *Journal of Materials Chemistry*, 2012, **22**, 5666-5675.
25. N. Saurín, J. Sanes and M. D. Bermúdez, *Tribol Lett*, 2014, **56**, 133-142.
26. Z. Wang, F. Li, J. Xia, L. Xia, F. Zhang, S. Bi, G. Shi, Y. Xia, J. Liu, Y. Li and L. Xia, *Biosensors and Bioelectronics*, 2014, **61**, 391-396.
27. L. T. Lim, R. Auras and M. Rubino, *Progress in Polymer Science*, 2008, **33**, 820-852.
28. K. K. Sadasivuni, D. Ponnamma, S. Thomas and Y. Grohens, *Progress in Polymer Science*, 2014, **39**, 749-780.
29. F. Tuinstra and J. L. Koenig, *The Journal of Chemical Physics*, 1970, **53**, 1126-1130.
30. S. Stankovich, D. A. Dikin, R. D. Piner, K. A. Kohlhaas, A. Kleinhammes, Y. Jia, Y. Wu, S. T. Nguyen and R. S. Ruoff, *Carbon*, 2007, **45**, 1558-1565.
31. T. Jiang, W. Liu, Y. Mao, L. Zhang, J. Cheng, M. Gong, H. Zhao, L. Dai, S. Zhang and Q. Zhao, *Chemical Engineering Journal*, 2015, **259**, 603-610.
32. V. Khare, M.-Q. Pham, N. Kumari, H.-S. Yoon, C.-S. Kim, J.-I. L. Park and S.-H. Ahn, *ACS Applied Materials & Interfaces*, 2013, **5**, 4063-4075.
33. N. Mathan, M. Arunjunairaj, T. Rajkumar, D. Ponraju and C. Vijayakumar, *J Therm Anal Calorim*, 2012, **110**, 1133-1141.
34. C. Maton, N. De Vos and C. V. Stevens, *Chemical Society Reviews*, 2013, **42**, 5963-5977.
35. D. Cai and M. Song, *Journal of Materials Chemistry*, 2010, **20**, 7906-7915.
36. D. Wang, Y. Bao, J.-W. Zha, J. Zhao, Z.-M. Dang and G.-H. Hu, *ACS Applied Materials & Interfaces*, 2012, **4**, 6273-6279.

37. C. Bao, L. Song, W. Xing, B. Yuan, C. A. Wilkie, J. Huang, Y. Guo and Y. Hu, *Journal of Materials Chemistry*, 2012, **22**, 6088-6096.

38. H. Gui, Y. Li, S. Chen, P. Xu, B. Zheng and Y. Ding, *Macromol. Res.*, 2014, **22**, 583-591.

39. M. Murariu, L. Bonnaud, P. Yoann, G. Fontaine, S. Bourbigot and P. Dubois, *Polymer Degradation and Stability*, 2010, **95**, 374-381.

40. C. Bao, L. Song, C. A. Wilkie, B. Yuan, Y. Guo, Y. Hu and X. Gong, *Journal of Materials Chemistry*, 2012, **22**, 16399-16406.

41. N. Hong, Y. Pan, J. Zhan, B. Wang, K. Zhou, L. Song and Y. Hu, *RSC Advances*, 2013, **3**, 16440-16448.

42. X. Wang, S. Zhou, W. Xing, B. Yu, X. Feng, L. Song and Y. Hu, *Journal of Materials Chemistry A*, 2013, **1**, 4383-4390.

43. S.-D. Jiang, Z.-M. Bai, G. Tang, Y. Hu and L. Song, *Industrial & Engineering Chemistry Research*, 2014, **53**, 6708-6717.

44. V. Katiyar, N. Gerds, C. B. Koch, J. Risbo, H. C. B. Hansen and D. Plackett, *Polymer Degradation and Stability*, 2010, **95**, 2563-2573.

45. S. Ran, Z. Guo, C. Chen, L. Zhao and Z. Fang, *Journal of Materials Chemistry A*, 2014, **2**, 2999-3007.

46. P. Lespade, R. Al-Jishi and M. S. Dresselhaus, *Carbon*, 1982, **20**, 427-431.

Content of Figures and Tables

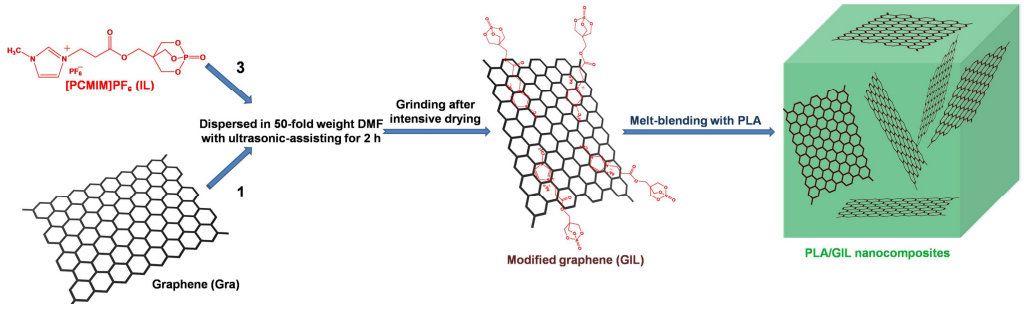

Fig. 1. Structures of [PCMIM]PF_6 and schematic diagrams of the preparation of PLA/GIL nanocomposite.

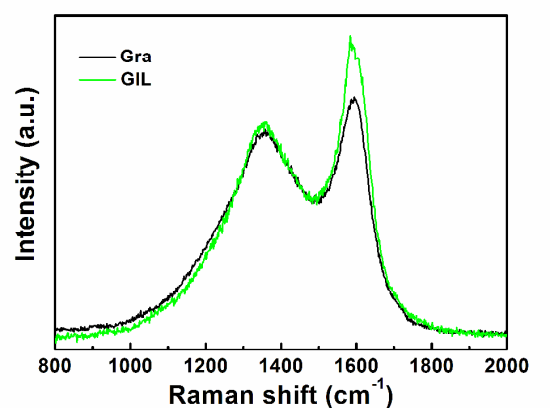

Fig. 2. Raman spectra of graphene and GIL.

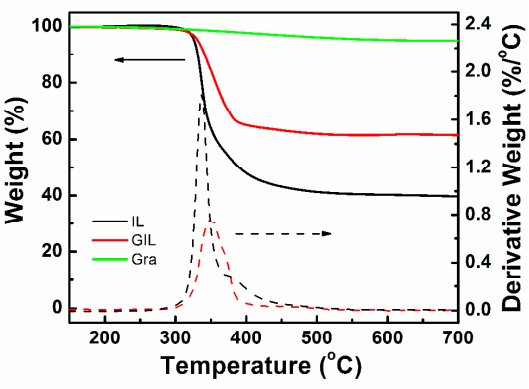

Fig. 3. TGA and DTG curves of IL and GIL under nitrogen condition.

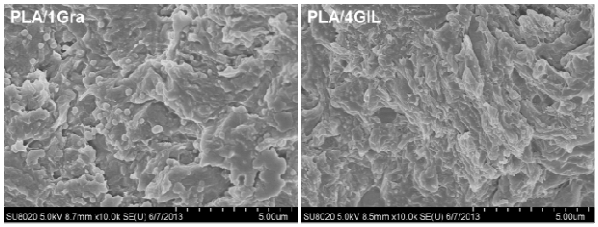

Fig. 4. FESEM images of fracture surface of PLA/1Gra and PLA/4GIL nanocomposites.

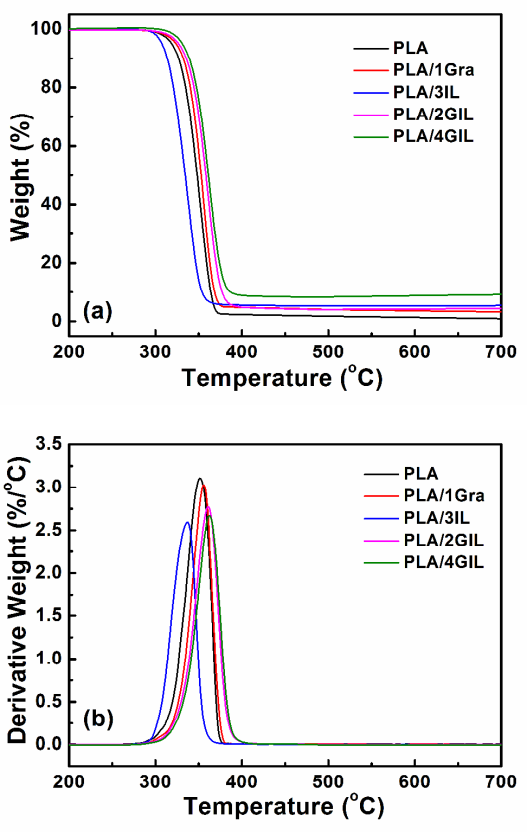

Fig. 5. (a) TGA and (b) DTG curves of PLA/Gra, PLA/IL and PLA/GIL nanocomposites.

5

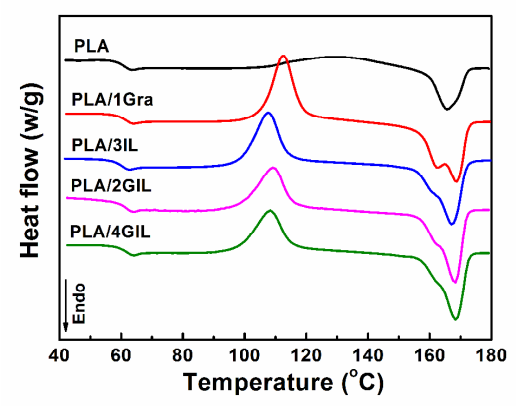

Fig. 6. DSC thermograms of different PLA nanocomposites.

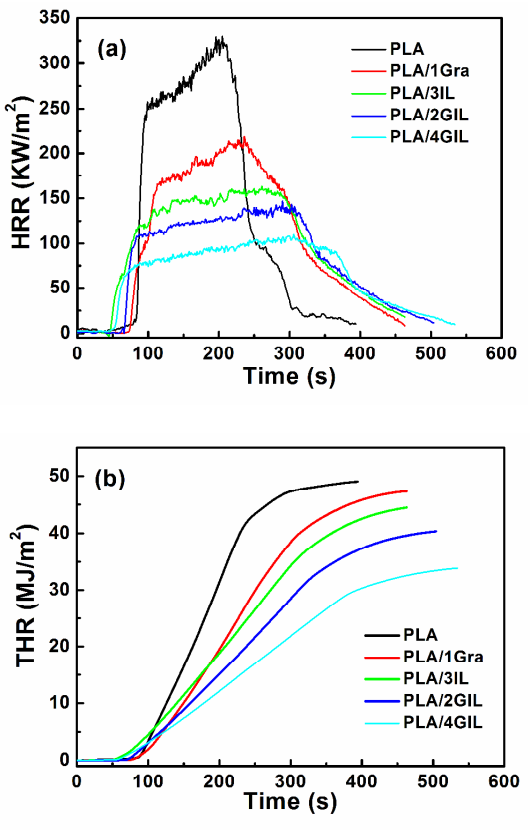

Fig. 7. (a) Heat release rate (HRR) and (b) total heat release (THR) curves for samples from cone calorimeter testing (CCT).

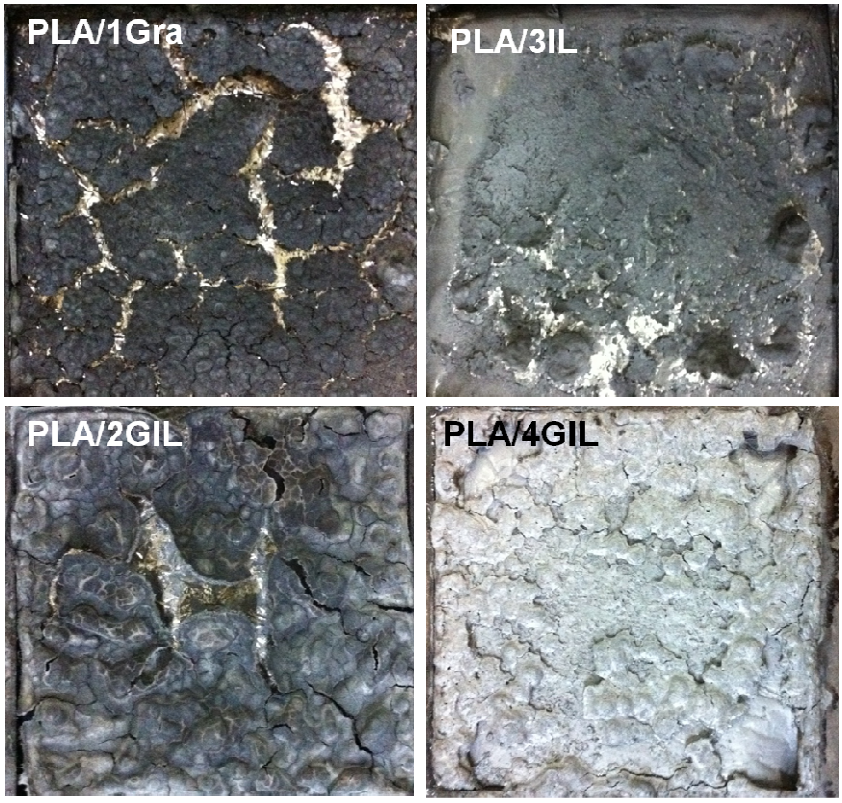

Fig. 8. Photos of the chars of PLA and PLA nanocomposites after CCT.

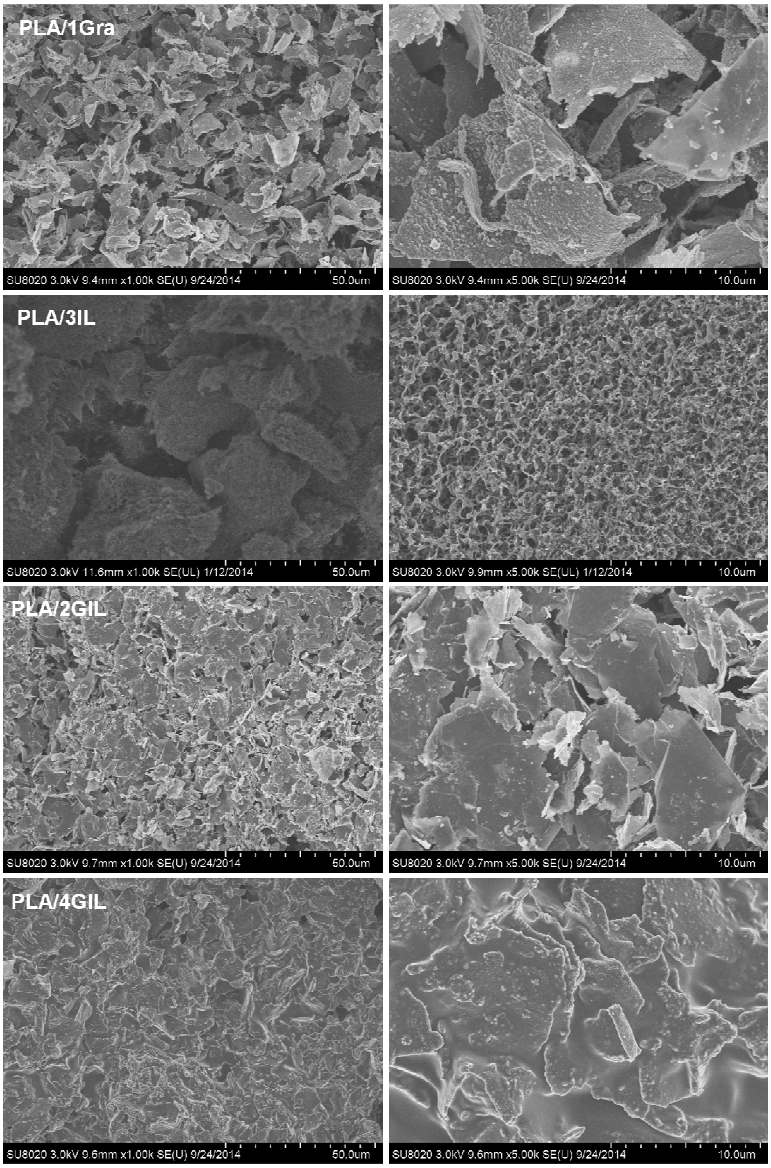

Fig. 9. FESEM image (50 μm and 10 μm) of char morphology surfaces of PLA nanocomposites after CCT.

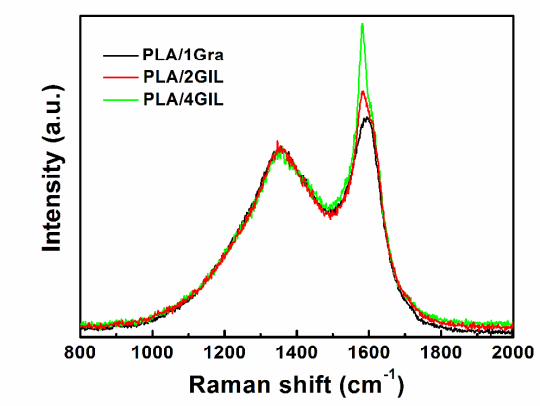

Fig. 10. Raman spectra of different samples after CCT.

Table 1 Thermal degradation and char residue data of all samples.

Sample	$T_{initial}$	T_{max}	Residue (*wt* %)	
			600 °C	700 °C
PLA	318.8	351.1	1.3	0.9
PLA/1Gra	324.9	356.1	2.4	3.4
PLA/3IL	307.5	335.8	5.4	5.3
PLA/2GIL	328.1	360.9	4.6	4.3
PLA/4GIL	331.4	364.5	9.2	9.0

Table 2 DSC data of PLA and PLA compositions

Sample	T_g (°C)	T_c (°C)	H_c (J/g)	T_{m1} (°C)	T_{m2} (°C)	H_m (J/g)	Crystallinity (%)
PLA	60.4	129.9	21.9	165.4	169.6	26.2	28.2
PLA/1Gra	61.3	112.3	20.5	162.6	169.1	30.2	32.5
PLA/3IL	58.6	107.7	20.8	162.0	167.1	29.5	31.7
PLA/2GIL	61.8	109.6	17.2	161.6	168.2	34.3	36.8
PLA/4GIL	62.2	108.8	15.5	160.7	168.0	34.7	37.3

The reported enthalpy value for PLA with 100% crystallinity is 93 $J \cdot g^{-1}$.[27]

Table 3 Mechanical properties of all samples.

Sample	Tensile strength (MPa)	Elongation at break (%)	Impac strength (kJ/m^2)
PLA	60 ± 1.2	5.3 ± 0.6	3.7 ± 0.9
PLA/1Gra	63 ± 1.7	4.9 ± 0.3	3.4 ± 0.3
PLA/3IL	57 ± 0.8	6.4 ± 0.7	4.6 ± 1.1
PLA/2GIL	61 ± 2.1	6.0 ± 1.3	4.1 ± 1.0
PLA/4GIL	62 ± 3.4	5.7 ± 1.5	4.3 ± 1.5

Table 4 Combustion parameters obtained from cone calorimeter

Sample	TTI (s)	t_p (s)	Av_{HRR} (kW/m^2)	p_{HRR} (kW/m^2)	THR (MJ/m^2)
PLA	88	205	150	324	49
PLA/1Gra	79	235	86	214	46
PLA/3IL	50	216	75	168	43
PLA/2GIL	68	285	67	141	40
PLA/4GIL	56	305	44	99	33

TTI: time to ignition; p_{HRR}: peak heat release rate; t_p: time to p_{HRR}; Av_{HRR}: average heat release rate; THR: total heal release.